Microelectronic Engineering 248 (2021) 111613

Contents lists available at ScienceDirect

Microelectronic Engineering

journal homepage: www.elsevier.com/locate/mee

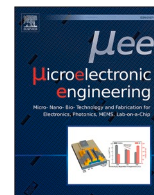

Diffusion-controlled growth of Cu thin films electrodeposited directly on atomic-layer-deposited WC diffusion barrier for Cu interconnect

Hongmin Youn [a], Sunjung Kim [a,*], Soo-Hyun Kim [b]

[a] School of Materials Science and Engineering, University of Ulsan, Ulsan 44610, Republic of Korea
[b] School of Materials Science and Engineering, Yeungnam University, Gyeongsan 38541, Republic of Korea

A R T I C L E I N F O

Keywords:
Electrodeposition
Cu thin film
Diffusion barrier
Diffusion-controlled deposition

A B S T R A C T

Direct copper (Cu) electrodeposition on a 10-nm atomic-layer-deposited (ALD) tungsten carbide (WC) diffusion barrier layer was investigated for building Cu interconnect in silicon (Si)-based microelectronic devices. The diffusion of Cu reducing species under potentiostatic Cu deposition was characterized according to applied cathodic potential in a neutral electrolyte with a concentration ratio of 1:10 for Cu to iminodiacetic acid (IDA) as a complexing agent. The diffusion-controlled nucleation and growth of Cu thin film on the ALD WC was figured out in relation to diffusion coefficients of Cu reducing species that were calculated from both modified current transient curves and more appropriately electrochemical impedance spectroscopy (EIS) analysis. At the end, the diffusion-controlled Cu fill of trenches with an aspect ratio of 6.3 and 15-nm bottom width was conducted by applying −1.4 V *vs* Ag/AgCl to an ALD-WC-covered, patterned Si wafer specimen.

1. Introduction

Aluminum (Al) had been used as an interconnect material for the silicon (Si)-based microelectronic devices in the past, but since IBM introduced the dual damascene process in 1997, copper (Cu) interconnect has become prevalent because the electrical resistivity of bulk Cu is 1.67 μΩ·cm, which is about 40% lower than 2.70 μΩ·cm of Al [1]. However, when Cu interconnect lines are built directly on a Si wafer, Cu atoms can degrade the performance of the microelectronic devices seriously by diffusing into SiO_2 and Si [2]. Therefore, a diffusion barrier layer which prevents Cu diffusion through SiO_2 and Si is required. For ultra large scale integration (ULSI) devices, trench and *via* structures have a very narrow width and a high aspect ratio, which make it challenging to deposit a diffusion barrier layer on SiO_2 with a good step coverage and then fill Cu without voids [3].

In this study, tungsten carbide (WC) was selected as a diffusion barrier material because it has the excellent mechanical and chemical stability, which is necessary for diffusion barriers [4]. Atomic layer deposition (ALD) was used to deposit a uniform, conformal WC diffusion barrier film over the highly integrated devices [5]. A Cu seed layer as an electrical conduction passage for a subsequent Cu electrodeposition, which has been conventionally formed on the top surface of a diffusion barrier layer, was not employed in order to allow more space inside trenches and vias for Cu fill [6]. Seedless Cu electrodeposition is advantageous for producing void- or defect-free Cu interconnect lines in the ULSI devices [7] as long as a dense, uniform growth of Cu thin film directly on a diffusion barrier surface is controlled on the nanometer scale. However, a large electrical resistivity of a 10-nm ALD WC diffusion barrier layer, which was measured as 366 μΩ·cm in this study, makes it difficult to electrodeposit Cu thin films directly on the ALD WC.

Fundamental approach of this study for seedless Cu electrodeposition on the 10-nm ALD WC diffusion barrier layer is to manipulate the diffusion-controlled nucleation and growth of Cu by adding iminodiacetic acid (IDA) as a complexing agent, which favors to form stable Cu-IDA complexes, to a neutral Cu electrolyte. Previous studies regarding direct Cu electrodeposition on various diffusion barriers have tried to achieve a uniform Cu growth using general electrochemical techniques, in which only the solution resistance, R_s is considered for Cu reduction behavior [8–16]. Most of them neglected that the polarization resistance, R_p, which exists in the interface between an electrolyte and a diffusion barrier, should be also considered to understand Cu electrodeposition as a diffusion-controlled reaction. Therefore, we investigated the influence of diffusion characteristics of Cu reducing species in the Cu/IDA electrolyte on the nucleation and growth of Cu on the ALD WC. Electrochemical impedance spectroscopy (EIS) was used to interpret diffusion-controlled Cu reduction considering both R_s and R_p of the

* Corresponding author.
E-mail address: sunjungkim@ulsan.ac.kr (S. Kim).

https://doi.org/10.1016/j.mee.2021.111613
Received 27 May 2021; Received in revised form 22 July 2021; Accepted 5 August 2021
Available online 13 August 2021
0167-9317/© 2021 Elsevier B.V. All rights reserved.

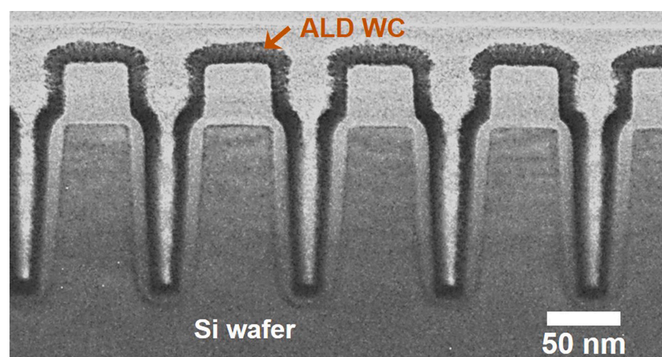

Fig. 1. Cross-sectional TEM image showing 10-nm ALD-WC-covered trenches of an aspect ratio of 6.3 and 15-nm bottom width in a Si wafer specimen [17].

electrochemical cell. Consequently, trenches with an aspect ratio of 6.3 and 15-nm bottom width, which were conformally covered with the 10-nm ALD WC layer, were attempted to fill with Cu under an optimized electrodeposition condition.

2. Experimental

2.1. Si wafer specimen preparation

A 10-nm thick WC diffusion barrier layer was deposited on a 6-in. Si wafer with a 50-nm thick SiO_2 layer using a shower-head type ALD reactor (Lucida-M100, NCD Technology) with a sequential supply of W $(CO)(CH_3CH_2C{\equiv}CCH_2CH_3)_3$ [tungsten tris(3-hexyne) carbonyl] contained in a canister kept at 80 °C and a N_2/H_2 mixture plasma as the reactant [17]. The WC layer was grown at 250 °C under a chamber pressure of approximately 0.5 Torr. The ratio of the N_2 and H_2 gas flow rates was 0.1 with a total reactant flow rate of 50 sccm (standard cubic centimeter per minute). The self-limited WC film growth were conducted at a precursor pulse of 10 s and a purge with 200 sccm of Ar for 10 s prior to a reactant pulsing. During the reactant pulsing of 15 s, a radio frequency power of 100 W was applied to the showerhead to ignite the corresponding plasma. After reactant pulsing, another purge step was performed for 10 s prior to the follow-up precursor pulse. A trench (bottom width: 15 nm) structure with an aspect ratio of 6.3 was consequently coated with a WC film of approximately 80% step coverage, as shown in Fig. 1. The electrical resistivity of the WC film, which consisted of 55 at.% W and 45 at.% C, was measured as 510 μΩ·cm.

The Si wafer was cut into rectangular specimens with a dimension of 2 × 1.5 cm prior to WC deposition. The surface of ALD WC layer was pretreated in a dilute HNO_3 solution, cleaned with ethanol, and rinsed with deionized water. Each wafer specimen was located inside a sealed working electrode, which was the aggregation of a conductive stainless steel structure, a rubber ring, a Teflon housing with an electrolyte-exposed area of 1.1 cm^2 and a Teflon cylinder with a Cu rod core. A pure Cu plate was used as a counter electrode, and an Ag/AgCl electrode was used as a reference electrode.

2.2. Materials and tools for Cu electrodeposition

An 500-ml aqueous electrolyte consisting of 0.01 M $CuSO_4{\cdot}5H_2O$ (Alfa Aesar) and 0.1 M $HN(CH_2COOH)_2$ (IDA; Sigma-Aldrich) was prepared, and its pH was adjusted to 7 using KOH solution (Daejung Chemical and Metals). The low Cu concentration compared with IDA ligand was determined to make the diffusion-controlled reduction of cupric ion or Cu-IDA complexes. Potentiostatic Cu electrodeposition on ALD WC in the Cu/IDA electrolyte was carried out for 100 s with varying applied potential from −1.0 to −1.6 V using a potentiostat (G750, Gamry Instruments) and a three-electrode cell. For the EIS analysis of Cu

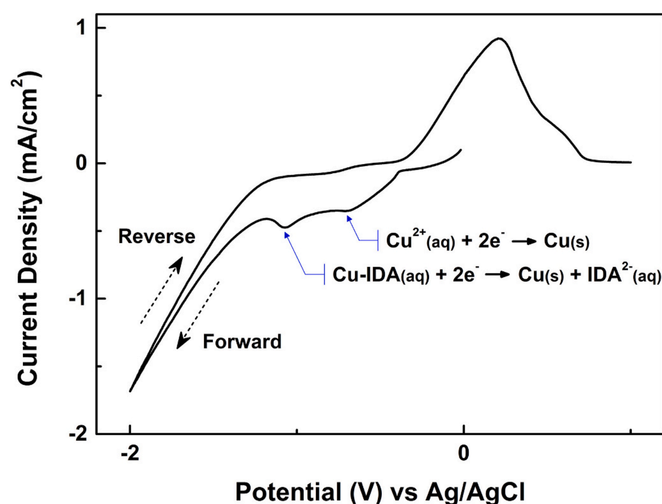

Fig. 2. Cyclic polarization curve in the Cu/IDA electrolyte of pH 7. Its scan rate is 10 mV/s.

electrodeposition on ALD WC at the same conditions, another potentiostat (IviumStat, Ivium Technologies) was also used. A frequency range for EIS was set to 10–10^7 Hz, and the impedance change with frequency was recorded under constant potential conditions.

2.3. Characterization of specimens

The growth morphology of Cu thin films on ALD WC was examined using a field emission scanning electron microscope (FE-SEM; Quanta 200, FEI) and an atomic force microscope (AFM; XE-100, Park Systems) in a non-contact mode. The AFM was also used to measure the surface roughness average, R_a of Cu deposits on ALD WC. The measurement of top projected areas of irregularly shaped Cu clusters was available using an image analysis software (Pixcavator IA, Intelligent Perception). The number of projected objects of a specific size range was automatically counted in the software. The sheet resistance of Cu layers on ALD WC was measured using a four-point probe (FPP-HS8, Dasol Eng.) in a dual configuration mode. A cross-section image of ALD-WC-covered trench structure was taken using a transmission electron microscopy (TEM; Tecnai F20 equipped with 200 kV accelerating voltage and field emission gun).

3. Results and discussion

3.1. Electrochemical deposition of Cu on ALD WC diffusion barrier

Fig. 2 shows a cyclic voltammogram in the Cu/IDA electrolyte while applied potential varied especially in the cathodic reaction region at a scan rate of 10 mV/s. Two distinguished local reduction peaks appeared around −0.7 and −1.0 V during forward potential scan. The peak near −0.7 V arises from a limited reduction current of cupric ions, Cu^{2+}, whereas another peak near −1.0 V characterizes the reduction of Cu-IDA complex to Cu deposit. Cu species in the Cu/IDA electrolyte of pH 7 prefers to form Cu-IDA complex by chelating with IDA ligand rather than to exist as free Cu^{2+} ion because the stability constant, log k of Cu-IDA complex is moderately as high as 10.55. If a stability constant of a metal-ligand complex is low, a chelation between a metal ion and a ligand is so weak to keep its complexing form. However, if a metal complexation with a ligand is too strong, a metal ion is difficult to reduce to metal by separating from the ligand when electrons are supplied to it [18]. Therefore, in this study, cathodic potentials larger than −1.0 V were applied to the ALD-WC-covered wafer specimens for the purposes of enhancing a proper separation of Cu-IDA complex into Cu^{2+} and IDA^{2-} and a simultaneous Cu reduction.

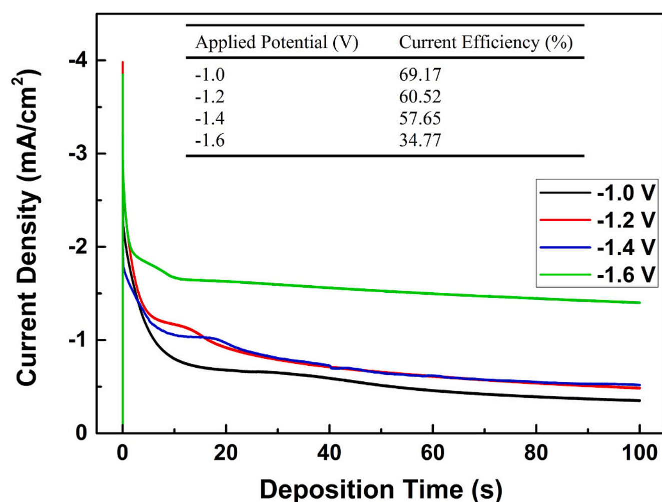

Fig. 3. Current transient curves for 100 s during potentiostatic deposition of Cu on ALD WC in the Cu/IDA electrolyte. The inserted table shows the current efficiency of Cu reduction according to applied potential.

Potentiostatic depositions of Cu on ALD WC were carried out for 100 s in the potential range of −1.0 to −1.6 V, as resultant current transient curves are shown in Fig. 3. The weight change of wafer specimens before and after Cu electrodeposition was measured five times and arithmetically averaged to calculate a practical deposition amount of Cu. A theoretical deposition amount was calculated using current transient curves in Fig. 3 and the following equation [11,12].

$$m = \frac{ItM}{nF} = \frac{A_{current\ transient}M}{nF} \tag{1}$$

where m is a theoretical deposition amount of Cu, I is a reduction current, t is a deposition time, M is an atomic weight, n is a number of electrons, F is the Faraday constant, and $A_{current\ transient}$ is an area under a current transient curve. A current efficiency of Cu electrodeposition on ALD WC could be simply calculated from practical and theoretical values of Cu deposition amount according to applied potential [11,13], as presented as an inserted table in Fig. 3. The current efficiency of Cu electrodeposition from Cu-IDA complex at −1.0 V was 69.17%. A previous study reported around 60% current efficiency for Cu^{2+} ion reduction [19]. As applied potential becomes more negative, current efficiency decreases gradually, and it drops as low as 34.77% especially for −1.6 V. In the cyclic voltammogram of Fig. 2, reduction current increased sharply beyond −1.2 V during the forward potential scan. It could be responsible for lowering current efficiency at larger cathodic potentials because hydrogen evolution becomes more violent and more competitive with Cu electrodeposition beyond −1.2 V.

3.2. Measurement of diffusion coefficients for potentiostatic Cu deposition

In this study, the diffusion-limited condition of Cu reduction was maintained by making the concentration ratio of Cu to IDA as 1:10 in the electrolyte. When the diffusion characteristic of Cu reducing species varies according to electrodeposition parameters such as applied cathodic potential, the nucleation and growth behavior of Cu on ALD WC can be influenced correspondingly. A rapid increase in reduction current at the early stage of Cu deposition on ALD WC, as shown in current transient curves in Fig. 3, is attributed to the initial nucleation of Cu on ALD WC. Subsequently, Cu deposition behavior enters a steady-state condition over time, which is governed by the diffusion of Cu reducing species such as Cu-IDA complex from the bulk electrolyte [8,10]. Therefore, investigating the relationship of diffusion coefficient and applied cathodic potential is useful to understand the growth behavior and resultant surface morphology of Cu thin films on ALD WC.

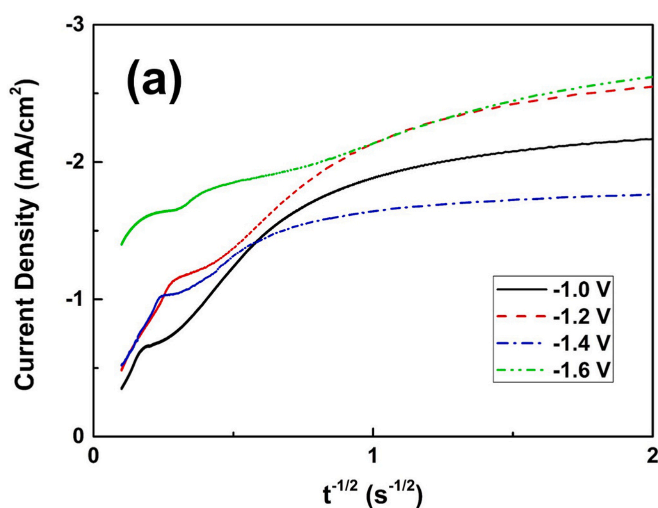

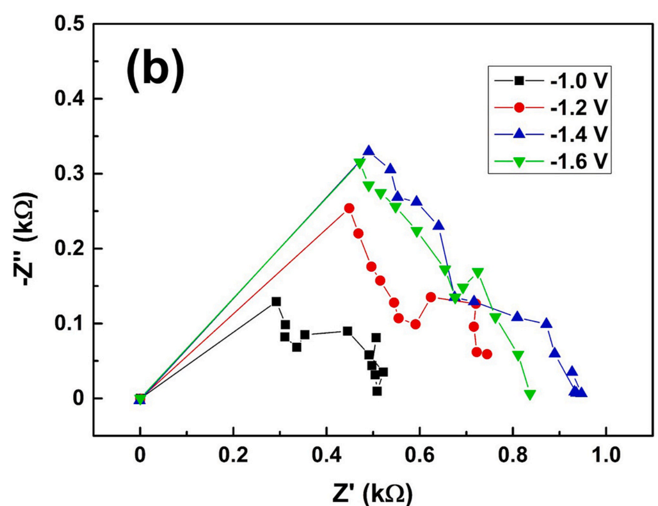

Fig. 4. (a) modified current transient curves based on the Cottrell equation. (b) Nyquist plots showing impedance change with applied potential in the frequency range of 10–10^7 Hz.

Table 1
Comparison of diffusion coefficients of Cu reduction, which were calculated respectively from the EIS analysis and the Cottrell equation using modified current transient curves, according to applied potential.

Applied potential (V)	Constant phase element, σ (s/Ω-cm^2)	Diffusion coefficient, D (cm^2/s × 10^{-7})	
		EIS	Current transient
−1.0	0.44	17.10	6.15
−1.2	0.57	6.71	6.77
−1.4	0.68	4.34	4.76
−1.6	0.67	4.60	3.38

The Cottrell equation, which is presented as below, was employed to calculate the diffusion coefficient of Cu reducing species as a function of applied potential by modifying the current transient curves (i-t curves) of Fig. 3 into the i-$t^{-1/2}$ curves [15,16,20], as shown in Fig. 4(a).

$$i = \frac{nFAC_0\sqrt{D}}{\sqrt{\pi t}} \tag{2}$$

where i is a current density, n is a number of electrons, F is the Faraday constant, A is an electrode surface area, C_0 is an initial concentration of

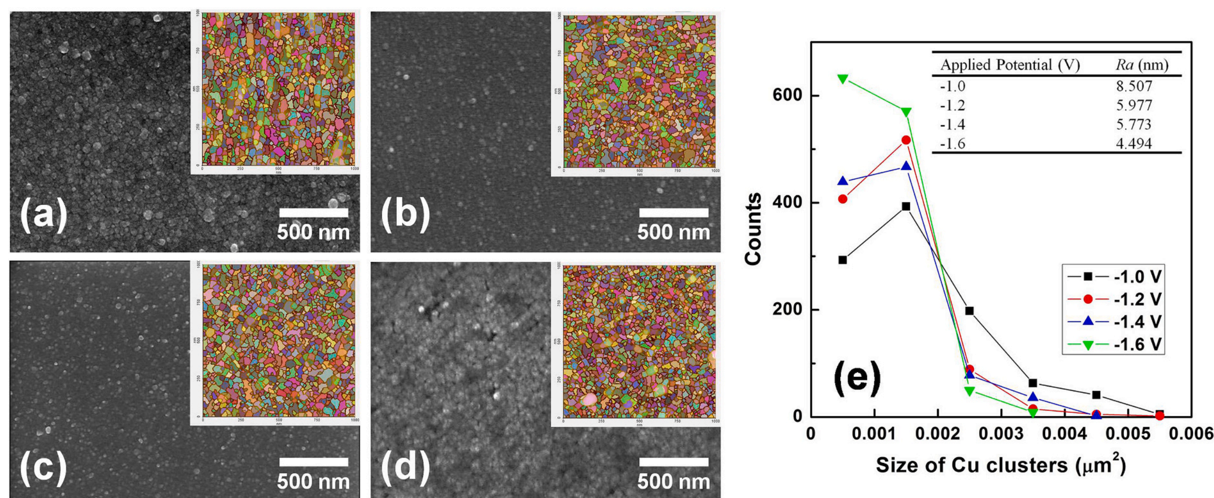

Fig. 5. Top-view SEM images of Cu thin films after 100-s deposition at (a) −1.0 V, (b) −1.2 V, (c) −1.4 V, and (d) −1.6 V, and their graphical conversions showing vertical projection areas of Cu clusters. (e) The variations in the size distribution of Cu clusters and the surface roughness, R_a of Cu thin films according to applied potential.

reducing species, t is a deposition time, and D is a diffusion coefficient. Front linear slopes of the i-$t^{-1/2}$ curves in Fig. 4(a), which describe diffusion characteristics under the steady-state Cu electrodeposition, were used to calculate the diffusion coefficients of Cu reducing species, as shown in Table 1. The diffusion coefficients calculated from the modified current transient curves tend to decrease with more negative potential, but their difference especially at low cathodic potentials does not appear considerable. The Cottrell equation assumes the diffusion behaviors of Cu reducing species when a steady-state reduction condition is reached after an initial period of Cu reduction. The equation includes a diffusion coefficient factor determined by considering the solution resistance, R_s of a bulk electrolyte; however, it is unclear whether it also take into account the polarization resistance, R_p, which, in this study, reflects the diffusion and reduction behavior of Cu-based species near the interface or electrical double layer between ALD WC and electrolyte. Thus, the EIS analysis of Cu electrodeposition on ALD WC in the Cu/IDA electrolyte was also conducted to measure diffusion coefficients because both R_s and R_p could be considered.

Fig. 4(b) shows Nyquist plots drawn by the EIS in the frequency range of 10–10^7 Hz according to applied potential. The Nyquist plots show a linear slope in the high frequency region (the left-hand side of the horizontal axis) and a hemispherical change in the low frequency region (the right-hand side of the horizontal axis), even though they include a considerable fluctuation in impedance with frequency change because a substantial evolution of hydrogen gas may hinder stable Cu reduction on the ALD WC cathode. The plots have a characteristic of Warburg impedance, which implies a diffusional impedance for electroactive species at high frequencies for a thin layer electrochemical cell, supposing the Randles equivalent circuit for electrochemical reactions [21–24]. The Warburg impedance can be simply expressed as $Z(\omega) = R_s + R_p$, where ω is an angular frequency, for this case. Thus, the linear slopes in the high frequency region of Fig. 4(b) represent the diffusion impedance of Cu reducing species considering both R_s and R_p, and accordingly can be used to determine a constant phase element, σ, which appears when an interfacial charging by electroactive species occurs near an electrode. Considering only the reduction of Cu-based species on the ALD WC cathode surface, the constant phase element can be written as the following equation including the diffusion coefficient of reduction, D_R.

$$\sigma = \frac{RT}{n^2F^2A\sqrt{2}} \cdot \frac{1}{\sqrt{D_R} \cdot C_R} \quad (3)$$

where R is the gas constant, and C_R is an impedance of reduction, which can be determined from the highest impedance of each Nyquist plot, W_{max}. Both constant phase element and diffusion coefficient of Cu reducing species calculated from the EIS analysis are shown with applied potential in Table 1. The variation in diffusion coefficients resulted from the EIS shows a clearer decreasing tendency with increasing cathodic potential in comparison with that obtained from the current transient curves. This relationship between applied potential and diffusion coefficient for Cu reduction can affect the diffusion rate of Cu reducing species like Cu-IDA complex, and resultantly the growth of Cu thin films. Larger current efficiency of Cu reduction at lower cathodic potential, as shown in Fig. 3, is also related with larger diffusion coefficient. Therefore, it is necessary to investigate how the diffusion characteristic of Cu reducing species varying with applied potential influences the growth and surface morphology of Cu thin films.

3.3. Morphological characterization of Cu thin film growth

Fig. 5 shows top-view SEM images of Cu thin films electrodeposited directly on ALD WC for 100 s according to applied potential, and their graphical conversion in order to reveal vertical projection areas of irregularly shaped Cu clusters. A relatively rough surface morphology of Cu thin film produced at −1.0 V is attributed to a faster diffusion of Cu reducing species toward the ALD WC cathode. In addition, the application of lower cathodic overpotential at −1.0 V to the electrically resistive 10-nm ALD WC layer could not activate Cu nucleation sites sufficiently. Therefore, Cu nuclei may form initially at a limited number of sites on ALD WC surface, and then further Cu reduction could prefer to occur on the top surface of pre-deposited Cu nuclei or clusters instead of creating new Cu nuclei [25,26]. This limited nucleation and growth behavior of Cu deposited at −1.0 V leads to relatively a rough, uneven surface of Cu thin film and a broad size distribution of Cu clusters, as seen in Fig. 5(e). Increasing applied potential up to −1.6 V results in a smoother surface morphology of Cu thin film. The size distribution of Cu clusters in Fig. 5(e) also shows that a greater number of smaller Cu nuclei are created when applying larger cathodic overpotentials to ALD WC. Cu nuclei grows as clusters hemispherically, and eventually merges each other laterally to form a complete Cu film before their further independent growth. The formation of denser Cu thin films consisting of smaller Cu clusters at larger cathodic potentials was influenced by slower Cu reduction and more chance of activating Cu nucleation sites over deposition time due to lower diffusion coefficients of Cu reducing species.

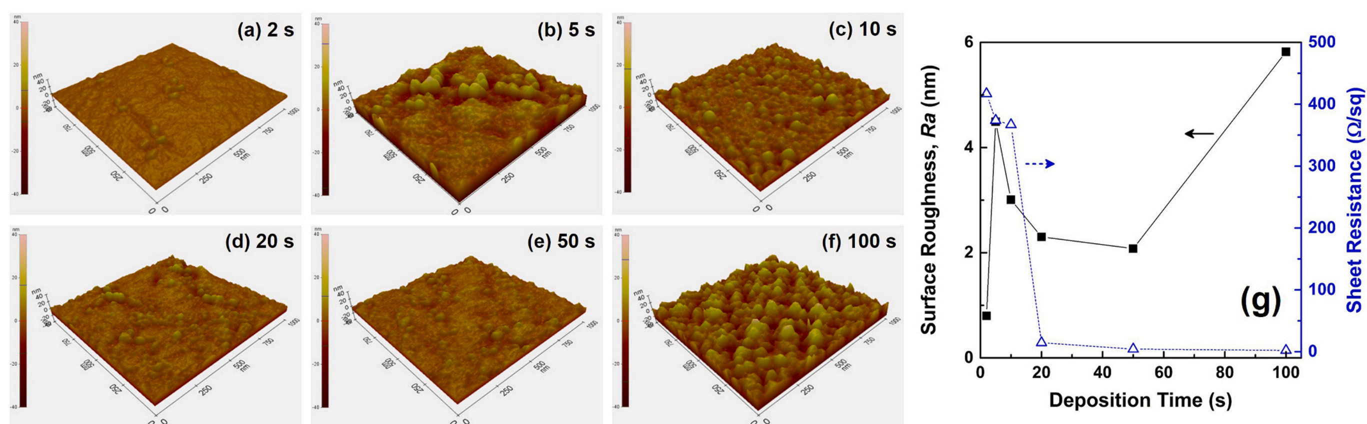

Fig. 6. (a-f) AFM images of Cu deposits over deposition time during potentiostatic deposition at −1.4 V. (g) The variations in the surface roughness, R_a and the sheet resistance of wafer specimens with Cu deposits according to deposition time.

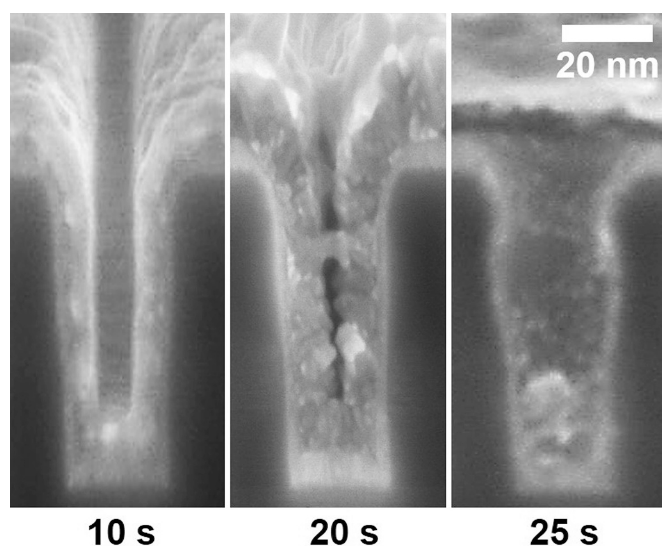

Fig. 7. Cross-sectional SEM image showing Cu fill of the trenches after 10-, 20-, and 25-s Cu electrodeposition at −1.4 V.

In order to figure out the nucleation and growth of Cu on ALD WC over time, we electrodeposited Cu on ALD WC at a constant potential of −1.4 V from 2 to 100 s. AFM images in Fig. 6 show the surface morphological evolution from Cu nucleation to the formation of a Cu thin film. However, investigating the variation in the surface roughness, R_a with deposition time, as shown in Fig. 6(g), is more appropriate to understand the progressive change of Cu deposit morphology. A very low R_a, 0.801 nm of a specimen processed for 2 s reflects mostly that of ALD WC layer because only a limited number of Cu nuclei are created at the early stage of Cu electrodeposition [25,26]. The surge of R_a in 5 s is attributed to the extensive formation and growth of separate Cu nuclei while most Cu nuclei are not in touch with each other laterally [9]. After the initial Cu nucleation growth period, part of growing Cu clusters are getting merged, resulting in a gradual decline of R_a up to 50 s. The formation of a Cu thin film is completed during this lateral coalescence of Cu clusters. The change of sheet resistance of the specimens in Fig. 6(g) also reveals the period of Cu film formation. Between 2 and 10 s, the sheet resistance decreases from 417 to 367 Ω/sq., which is highly influenced by the ALD WC layer since growing Cu nuclei or clusters are still isolated. However, it drops sharply to 14.5 Ω/sq. after 20-s electrodeposition, indicating that most Cu clusters are merged each other with forming a film. As a Cu film thickens subsequently with deposition time, a further decrease in the sheet resistance is observed. Likewise, a rapid increase of R_a after 50 s is brought about by a continuous growth of a Cu thin film.

A patterned Si wafer specimen with trenches of an aspect ratio of 6.3 and 15-nm bottom-width was provided from one of major chip manufacturers, and an ALD WC layer was deposited conformally along with the wall of trenches, as seen in the TEM image of Fig. 1. As previously used to deposit a Cu thin film in Fig. 6, −1.4 V was applied to the ALD WC cathode of the patterned wafer specimen for 10, 20, and 25 s in the Cu/IDA electrolyte. Fig. 7 shows the consequent Cu fill within trenches. Mechanical elongation of Cu deposits, which was induced while cutting the wafer specimen in order to expose the cross-section of trenches, also appears in Fig. 7. Cu fill was completed due to the continuous growth of Cu thin film simultaneously from the sidewalls and bottom of trenches. The conformal growth behavior of Cu thin film with electrodeposition time could be attributed to the diffusion-controlled nucleation and growth of Cu on ALD WC, which was previously verified from both modified current transient curves and EIS analysis during Cu reduction.

4. Conclusion

Diffusion-controlled Cu electrodeposition condition was developed using IDA as a Cu complexing agent in a neutral Cu/IDA electrolyte in order to deposit Cu thin films directly on electrically resistive 10-nm ALD WC diffusion barrier layer. Diffusion characteristic of Cu reducing species like Cu-IDA complex was dependent on applied cathodic potential, which varied from −1.0 to −1.6 V. Both modified current transient curves and more appropriately Nyquist plots obtained from EIS analysis were used to determine the diffusion coefficient of Cu reducing species at each applied potential. As applied potential became more negative, the diffusion of Cu reducing species got slower with producing denser, more uniform Cu thin films. Finally, Cu fill of ALD-WC-covered trenches with an aspect ratio of 6.3 was conducted by applying −1.4 V, at which both diffusion coefficient and current efficiency were proper for thin, smooth Cu film formation, to the patterned wafer specimen.

Declaration of Competing Interest

The authors declare that they have no known competing financial interests or personal relationships that could have appeared to influence the work reported in this paper.

Acknowledgement

This work was supported by the 2019 Research Fund of University of

Ulsan.

References

[1] O. Chyan, T.N. Arunagiri, T. Ponnuswamy, Electrodeposition of copper thin film on ruthenium: a potential diffusion barrier for Cu interconnects, J. Electrochem. Soc. 150 (2003) C347, https://doi.org/10.1149/1.1565138.

[2] H. Ono, T. Nakano, T. Ohta, Diffusion barrier effects of transition metals for Cu/M/Si multilayers (M=Cr, Ti, Nb, Mo, Ta, W), Appl. Phys. Lett. 64 (1994) 1511, https://doi.org/10.1063/1.111875.

[3] M. Hasegawa, Y. Okinaka, Y. Shacham-Diamand, T. Osaka, Void-free trench-filling by electroless copper deposition using the combination of accelerating and inhibiting additives, Electrochem. Solid-State Lett. 9 (2006) C138, https://doi.org/10.1149/1.2206008.

[4] S.J. Wang, H.Y. Tsai, S.C. Sun, M.H. Shiao, Thermal stability of sputtered tungsten carbide as diffusion barrier for copper metallization, J. Electrochem. Soc. 148 (2001) G500, https://doi.org/10.1149/1.1386644.

[5] M. Leskelä, M. Ritala, Atomic layer deposition (ALD): from precursors to thin film structures, Thin Solid Films 409 (2002) 138, https://doi.org/10.1016/S0040-6090(02)00117-7.

[6] B. Im, S. Kim, Influence of additives on Cu thin films electrodeposited directly on Ti diffusion barrier in Cl^--free electrolytes for Cu interconnect, Microelectron. Eng. 172 (2017) 8, https://doi.org/10.1016/j.mee.2017.02.006.

[7] D. Grujicic, B. Pesic, Reaction and nucleation mechanisms of copper electrodeposition from ammoniacal solutions on vitreous carbon, Electrochim. Acta 50 (2005) 4426, https://doi.org/10.1016/j.electacta.2005.02.012.

[8] A. Hauch, A. Georg, Diffusion in the electrolyte and charge-transfer reaction at the platinum electrode in dye-sensitized solar cells, Electrochim. Acta 46 (2001) 3457, https://doi.org/10.1016/S0013-4686(01)00540-0.

[9] D. Grujicic, B. Pesic, Electrodeposition of copper: the nucleation mechanisms, Electrochim. Acta 47 (2002) 2901, https://doi.org/10.1016/S0013-4686(02)00161-5.

[10] M.B. Vukmirovic, N. Vasiljevic, Diffusion-limited current density of oxygen reduction on copper, J. Electrochem. Soc. 150 (2003) B10, https://doi.org/10.1149/1.1526554.

[11] B.D. Adams, C. Radtke, R. Black, M.L. Trudeau, K. Zaghib, L.F. Nazar, Current density dependence of peroxide formation in the Li–O_2 battery and its effect on charge, Energy Environ. Sci. 6 (2013) 1772, https://doi.org/10.1039/C3EE40697K.

[12] M.E. Straumanis, M. Dutta, The divalency of tin ions formed during anodic dissolution and the behavior of the tin anode, Inorg. Chem. 5 (1966) 992, https://doi.org/10.1021/ic50040a009.

[13] J. Iniesta, P.A. Michaud, M. Panizza, G. Cerisola, A. Aldaz, C. Comninellis, Electrochemical oxidation of phenol at boron-doped diamond electrode, Electrochim. Acta 46 (2001) 3573, https://doi.org/10.1016/S0013-4686(01)00630-2.

[14] J.M.E. Harper, C. Cabral, P.C. Andricacos, L. Gignac, I.C. Noyon, K.P. Rodbell, C. K. Hu, Mechanisms for microstructure evolution in electroplated copper thin films near room temperature, J. Appl. Phys. 86 (1999) 2516, https://doi.org/10.1063/1.371086.

[15] N. Koura, T. Tsukamoto, H. Shoji, T. Hotta, Preparation of various oxide films by an electrophoretic deposition method: a study of the mechanism, Jpn. J. Appl. Phys. 34 (1995) 1643, https://doi.org/10.1143/JJAP.34.1643.

[16] L. Heerman, A. Tarallo, Theory of the chronoamperometric transient for electrochemical nucleation with diffusion-controlled growth, J. Electroanal. Chem. 470 (1999) 70, https://doi.org/10.1016/S0022-0728(99)00221-1.

[17] J.B. Kim, S.-H. Kim, W.S. Han, D.-J. Lee, Atomic layer deposited nanocrystalline tungsten carbides thin films as a metal gate and diffusion barrier for Cu metallization, J. Vac. Sci. Technol. A 34 (4) (2016), 041504, https://doi.org/10.1116/1.4951691.

[18] H.E. Lundager Madesen, H.H. Christensen, C. Gottlieb-Petersen, Stability constants of copper(II), zinc, manganese(II), calcium, and magnesium complexes of N-(phosphonomethyl) glycine (glyphosate), Acta Chem. Scand. A 32 (1978) 79, https://doi.org/10.3891/acta.chem.scand.32a-0079.

[19] J.-M. Quemper, E. Dufour-Gergam, N. Frantz-Rodriguez, J.-P. Gilles, J.-P. Grandchamp, A. Bosseboeuf, Effects of direct and pulse current on copper electrodeposition through photoresist molds, J. Micromech. Microeng. 10 (2000) 116, https://doi.org/10.1088/0960-1317/10/2/303.

[20] D.P. Valencia, F.J. Gonzalez, Understanding the linear correlation between diffusion coefficient and molecular weight. A model to estimate diffusion coefficients in acetonitrile solutions, Electrochem. Commun. 13 (2011) 129, https://doi.org/10.1016/j.elecom.2010.11.032.

[21] Q. Wang, J.-E. Moser, M. Grätzel, Electrochemical impedance spectroscopic analysis of dye-sensitized solar cells, J. Phys. Chem. B 109 (2005) 14945, https://doi.org/10.1021/jp052768h.

[22] R. Kern, R. Sastrawan, J. Ferber, R. Stangl, J. Luther, Modeling and interpretation of electrical impedance spectra of dye solar cells operated under open-circuit conditions, Electrochim. Acta 47 (2002) 4213, https://doi.org/10.1016/S0013-4686(02)00444-9.

[23] A.-C. Ciubotariu, L. Benea, M. Lakatos-Varsanyi, V. Dragan, Electrochemical impedance spectroscopy and corrosion behaviour of Al_2O_3–Ni nano composite coatings, Electrochim. Acta 53 (2008) 4557, https://doi.org/10.1016/j.electacta.2008.01.020.

[24] M. Adachi, M. Sakamoto, J. Jiu, Y. Ogata, S. Isoda, Determination of parameters of electron transport in dye-sensitized solar cells using electrochemical impedance spectroscopy, J. Phys. Chem. B 110 (2006) 13872, https://doi.org/10.1021/jp061693u.

[25] J.A. Venables, G.D.T. Spiller, M. Hanbücken, Nucleation and growth of thin films, Rep. Prog. Phys. 47 (1984) 399, https://doi.org/10.1088/0034-4885/47/4/002.

[26] N. Eliaz, M. Eliyahu, Electrochemical processes of nucleation and growth of hydroxyapatite on titanium supported by real-time electrochemical atomic force microscopy, J. Biomed. Mater. Res. A 80 (2007) 621, https://doi.org/10.1002/jbm.a.30944.